THE JOURNAL OF BIOLOGICAL CHEMISTRY VOL. 281, NO. 47, pp. 36327–36337, November 24, 2006

An Archaeal Peptidase Assembles into Two Different Quaternary Structures

A TETRAHEDRON AND A GIANT OCTAHEDRON[*][S]

Received for publication, May 9, 2006, and in revised form, August 3, 2006 Published, JBC Papers in Press, September 14, 2006, DOI 10.1074/jbc.M604417200

Guy Schoehn[‡1], **Frédéric M. D. Vellieux**[§1], **M. Asunción Durá**[§1,2], **Véronique Receveur-Bréchot**[¶], **Céline M. S. Fabry**[‡], **Rob W. H. Ruigrok**[‡], **Christine Ebel**[§], **Alain Roussel**[¶3], **and Bruno Franzetti**[§4]

From the [‡]*Laboratoire de Virologie Moléculaire et Structurale c/o EMBL, FRE 2854 CNRS-UJF, 38042 Grenoble,* [§]*Laboratoire de Biophysique Moléculaire, Institut de Biologie Structurale J.-P. Ebel, UMR 5075 CNRS-CEA-UJF, 38027 Grenoble, and* [¶]*Architecture et Fonction des Macromolécules Biologiques, UMR 6098 CNRS, Universités Aix-Marseille I and II, 13288 Marseille, France*

Cellular proteolysis involves large oligomeric peptidases that play key roles in the regulation of many cellular processes. The cobalt-activated peptidase TET1 from the hyperthermophilic Archaea *Pyrococcus horikoshii* (PhTET1) was found to assemble as a 12-subunit tetrahedron and as a 24-subunit octahedral particle. Both quaternary structures were solved by combining x-ray crystallography and cryoelectron microscopy data. The internal organization of the PhTET1 particles reveals highly self-compartmentalized systems made of networks of access channels extended by vast catalytic chambers. The two edifices display aminopeptidase activity, and their organizations indicate substrate navigation mechanisms different from those described in other large peptidase complexes. Compared with the tetrahedron, the octahedron forms a more expanded hollow structure, representing a new type of giant peptidase complex. PhTET1 assembles into two different quaternary structures because of quasi-equivalent contacts that previously have only been identified in viral capsids.

Cytosolic proteolysis is a key cellular process. In addition to its role in amino acid metabolism, it is responsible for protein quality control and the adjustment of the turnover of regulatory molecules (1, 2). Initial proteolysis is carried out by nonspecific endoproteases (1). Through oligomerization, these enzymes form barrel-like cellular subcompartments to protect cytoplasmic proteins from unwanted cleavage; the active sites are situated in proteolytic chambers, only accessible to unfolded polypeptides. In Eukarya and Archaea, the 20 S proteasome is the core of this proteolytic system (3, 4). The proteins to be degraded are unfolded and translocated into the proteolytic complex by energy-dependent regulatory particles (5). Polypeptide degradation results in multiple endoproteolytic cleavage, yielding short peptides (6–12 residues in length) (6). The final breakdown of these fragments is probably achieved by a collection of ATP-independent exopeptidases, which have been proposed to be essential components of the protein degradation system (7, 8).

Structural studies on the Tricorn protease complex, an archaeal carboxypeptidase (peptidyl-di/tripeptidase), have shown that some exopeptidases can also form multimeric ring structures, with the active sites sequestered within an internal chamber (9). This feature of compartmentalization was also recognized in the three-dimensional structures of three ATP-independent intracellular aminopeptidases: Gal6, leucine aminopeptidase, and the D-aminopeptidase DppA (10–12). In eukaryotic cells, the tripeptidyl-peptidase II also forms a giant, well organized toroidal oligomeric structure (13). All these exopeptidases could function as scavengers of the oligopeptides generated by the ATP-dependent endoproteases (14).

TET is another type of a large hollow peptidase complex. It was characterized initially in the halophilic Archaea *Haloarcula marismortui* (15). The complex has a tetrahedral shape and is a broad substrate specificity aminopeptidase capable of degrading large peptides. In the MEROPS peptidase data base (16), TET belongs to the M42 family of metallopeptidases (clan MH).

Pyrococcus horikoshii is an anaerobic Archaea, which grows optimally at 98 °C. It was isolated from hydrothermal fluid samples obtained at a depth of 1395 m in the Pacific Ocean (17). We recently showed that the *P. horikoshii* TET2 protein (PhTET2),[5] which shares 24% identity with the HmTET, is a 12-subunit tetrahedral aminopeptidase that

* This work was supported in part by the Groupement d'Intérêt Scientifique Génomique Marine (Roscoff-France). The costs of publication of this article were defrayed in part by the payment of page charges. This article must therefore be hereby marked "*advertisement*" in accordance with 18 U.S.C. Section 1734 solely to indicate this fact.

The atomic coordinates and structure factors (code 2CF4) have been deposited in the Protein Data Bank, Research Collaboratory for Structural Bioinformatics, Rutgers University, New Brunswick, NJ (http://www.rcsb.org/).

Density maps have been deposited in the Macromolecular Structure Database with accession numbers 1188 for PhTET1-12s and 1189 for PhTET1-24s.

[S] The on-line version of this article (available at http://www.jbc.org) contains supplemental Figs. 1–3 and Movies 1 and 2.

[1] These authors equally contributed to this work.

[2] Supported by a Marie Curie Intra-European Fellowship (European Community Sixth Framework Programme).

[3] Present address: Centre de Biophysique Moléculaire, 45071 Orléans, France.

[4] To whom correspondence should be addressed: Laboratoire de Biophysique Moléculaire, Institut de Biologie Structurale J.-P. Ebel, UMR 5075 CEA-CNRS-UJF, 41 Rue Jules Horowitz, 38027 Grenoble Cedex 1, France. Tel.: 33-4-38-78-95-69; Fax: 33-4-38-78-54-94; E-mail: franzetti@ibs.fr.

[5] The abbreviations used are: PhTET2, *P. horikoshii* TET2; HmTET, *Haloarcula marismortui* TET; PhTET1-12s, *P. horikoshii* TET1 12-subunit complex; PhTET1-24s, *P. horikoshii* TET1 24-subunit complex; PIPES, piperazine-*N*,*N*′-bis(2-ethanesulfonic acid); *p*NA, 4-nitroaniline; AMC, 7-amino-4-methylcoumarin; AAP, *V.* (formerly *Aeromonas*) *proteolyticus* aminopeptidase; HPLC, high pressure liquid chromatography.

displays a nonprocessive catalytic activity against N-terminal aliphatic and neutral amino acids (18). The structure of the PhTET2 edifice reveals the self-compartmentalizing nature of the complex (19, 20). In the genome of *P. horikoshii,* the open reading frame PH0519 encodes a homolog of PhTET2 that has been characterized as a cobalt-activated peptidase, suspected to be a deblocking aminopeptidase and thereby named DAP (21). The three-dimensional structures of PH0519, presented here, show that it can assemble alternatively as a tetrahedral dodecameric particle (therefore called PhTET1-12s) or as an octahedral tetracosameric edifice (PhTET1-24s). These assemblies are different from those observed in the other self-compartmentalized protease complexes of known three-dimensional structures. A mechanism of action for PhTET1 based on its peculiar compartmentalization and structural features is proposed.

EXPERIMENTAL PROCEDURES

Protein Expression, Purification, and Crystallization

The expression of the PH0519 protein from *P. horikoshii* in *Escherichia coli*, its purification, and the crystallization conditions are described elsewhere (22).

Electron Microscopy

Generation of the Model—We started with images obtained by negatively staining a PhTET1 sample with sodium silicotungstate, pH 7.5. Two different types of particles were observed. The images of the smaller particle were similar to the images of halophilic TET aminopeptidase (15). For the larger particle, at least two different characteristic views are easy to recognize: one ring made by six spots of density and a wheel-like structure (Fig. 1*A*). Two-dimensional averaging of 20 particles from each type, respectively, exhibit 3- and 4-fold symmetry axes. To generate a starting three-dimensional model, the same technique as described previously (15) was used but starting with the two-dimensional averages shown in Fig. 1*A*.

Cryoelectron Microscopy—Grids were prepared as described (23) and observed with a GATAN cryotransfer stage on a Philips CM200 LaB6 microscope at 200 kV. Images were recorded on Kodak SO 163 film under low dose conditions ($<10\ e^{-}/Å^{2}$) at a nominal magnification of 50,000 times with defocus values between 1.2 and 2.5 μm. Good micrographs were digitized on a Zeiss Photoscan TD scanner with a pixel size of 14 μm (2.8 Å $pixel^{-1}$). Using x3d (24), 11,400 small particles and 8,500 big particles from 15 images were selected and interactively boxed into 128 $\times$ 128 pixel boxes. These images were then corrected for the contrast transfer function as described (15). The structures of both particles were determined using a projection matching method implemented in SPIDER (15, 25). The starting models were, respectively, the three-dimensional structure of HmTET (15) and the octahedral particle determined using negative staining (see below). For the tetrahedral particle, 159 orientations equally distributed in the tetrahedral asymmetric unit (15) were used, and for the octahedral form, 58 different projections covering 1/24 of the space. The refinement (projection matching) was carry out using the phase flipped data set until no further changes were visible in the map (100 cycles for PhTET1-12s and 50 cycles for PhTET1-24s). The final reconstructions were calculated by back projection using the fully contrast transfer function corrected set of images and selecting about 75% of the images that had the highest correlation coefficient against the reprojections of the model (PhTET1-12s, 8,000 particles; PhTET1-24s, 6,000 images). The resolution of the two maps (PhTET1-12s, 14 Å; PhTET1-24s, 15 Å) was determined by splitting the data randomly into two halves and by comparing the resulting reconstructions by Fourier Shell Correlation (26) at 0.3 level (see Supplemental Material and supplemental Fig. 1).

Diffraction Data Collection and Structure Determination of PhTET1-12s

X-ray diffraction data were collected from a single selenium-substituted PhTET1-12s crystal on the ID14-4 beam line at the European Synchrotron Radiation Facility. The data frames were processed with XDS (27) and further processed and scaled using SELDAT, SCALKB2, and KBAPLY from the BioMol software suite.[6] While structure determination was being attempted using the MAD method, a structural model became available in the Protein Data Bank with the three-dimensional structure of *Bacillus subtilis* YsdC[7] (Protein Data Bank code 1VHE). This protein shares 36.3% sequence identity with the PhTET1 subunit. The three-dimensional structure of PhTET1-12s was solved at 3.1 Å resolution by molecular replacement (28). The calculations were performed with PHASER (29) using all available diffraction data. The molecular replacement solution has a *Z* value of 9.62, a log-likelihood gain value of 35.93, and a proper packing inside the F4(1)32 cell, which shows the arrangement of the PhTET1-12s subunits into tetrahedral homo-dodecameric particles. Model refinement is described in the Supplemental Material. The refined model has residual indices $R_f = 25.6\%$ and cross-validation *R*free = 33.1%, together with satisfactory geometry. Statistics of data collection and processing, model refinement, and model geometry are listed in the supplemental Table 1. Model quality and stereochemistry were checked using CNS (30) and PROCHECK (31). Molecular surfaces and electrostatic potentials were computed using Adaptive Poisson-Boltzmann Solver (32). The figures were prepared with PyMOL (33).

Quasi-atomic Models

Docking the dodecamer obtained by x-ray into the tetrahedral particle was done with SITUS (34) (unique result with a cross-correlation coefficient of 0.35). The fitting into the octahedral particle was done using URO (35) as described (23). The x-ray structure of one monomer was manually placed into the density corresponding to one monomer of the octahedral EM map that makes up the asymmetric unit. URO (35) was used to generate a preliminary quasi-atomic model of the octahedral particle by applying all the internal symmetries. The optimization procedure was also performed by using URO (35). The quality of the final fit is given by a correlation coefficient of 0.98,

[6] Groningen Protein Crystallography Group, unpublished data.
[7] Structural GenomiX Inc., San Diego, unpublished results.

a crystallographic *R* factor of 16.2% and a quadratic misfit of 1.3. The fitted scale factor was 0.91.

PhTET1 Activity Assays

PhTET1 hydrolytic activity was determined as follows. Reactions were initiated by addition of the enzyme (5 μg/ml, in the case of PhTET1-12s, or 10 μg/ml, for PhTET1-24s) to a prewarmed mixture containing the potential substrate in 50 mM PIPES, 150 mM KCl, 1 mM $CoSO_4$, pH 7.5, and covered by a layer of mineral oil to avoid water evaporation. Incubations were performed at 90 °C. To measure the evolution of the quantity of amino acids and di- and tripeptides in the reaction mixture, 80-μl aliquots were removed from the reaction mixture at 5-min intervals and added to 200 μl of cold acetonitrile to stop the reaction and precipitate the protein, which was separated by centrifugation. Two hundred fifty microliters of supernatant were dried under vacuum. Solids were dissolved in the same volume of Beckman analysis buffer, and the amino acids and small peptides present in each sample were quantified on a model 7300 Beckman amino acid analyzer, using the standard sodium citrate elution buffer system. To follow the progress of peptidyl- and aminoacyl-*p*NA compounds in the reaction mixture, the solids remaining after drying were dissolved in 125 μl of chromatography initial solvent (eluent A). Fifty microliters were injected on a μRPC C2/C18 ST column (4.6 × 100 mm) (Amersham Biosciences) in an ÄKTA purifier system (Amersham Biosciences). Chromatographic conditions were dependent of the peptide mixture, but in all cases eluent A contained 0.065% (v/v) trifluoroacetic acid and 2% (v/v) acetonitrile in water, and eluent B contained 0.05% (v/v) trifluoroacetic acid in 80% (v/v) acetonitrile. Flow was adjusted at 0.5 ml/min, and runs were carried out at room temperature. Calibrations were made by using authentic standards. Each sample was accompanied by an appropriate enzyme blank. Direct assay of generated *p*NA and AMC is described in the Supplemental Material.

RESULTS

Cryoelectron Microscopy Revealed Tetrahedral and Octahedral Hollow Particles—In gel filtration, the PhTET1 protein yields two peaks with apparent molecular masses of 400 and 800 kDa, respectively (22). Analytical ultracentrifugation studies, performed on the partially purified complexes, showed that in addition to a particle with a sedimentation coefficient $s_{20,w}$ of 15 S, *i.e.* the same value as dodecameric PhTET2 (18), a large PhTET1 particle was present. This particle displayed an $s_{20,w}$ of 23 S, consistent with an assembly of 24 subunits (results not shown).

The PhTET1 complexes were analyzed by negative staining electron microscopy showing two populations of homogeneous particles (Fig. 1*A*). Cryoelectron microscopy images were obtained, and their respective quaternary structures were determined by image analysis and three-dimensional reconstruction. The three-dimensional structures of the tetrahedral and octahedral particles, at resolutions of ~15 Å, are shown in Fig. 1*C*, *left* and *right panel*, respectively. The 12-subunit assembly is a tetrahedron of largest dimension of ~134 Å, which is similar to the HmTET protease (15) and to the TET2 homolog from *P. horikoshii* (18–20). Four 20 Å openings (called 3f) are

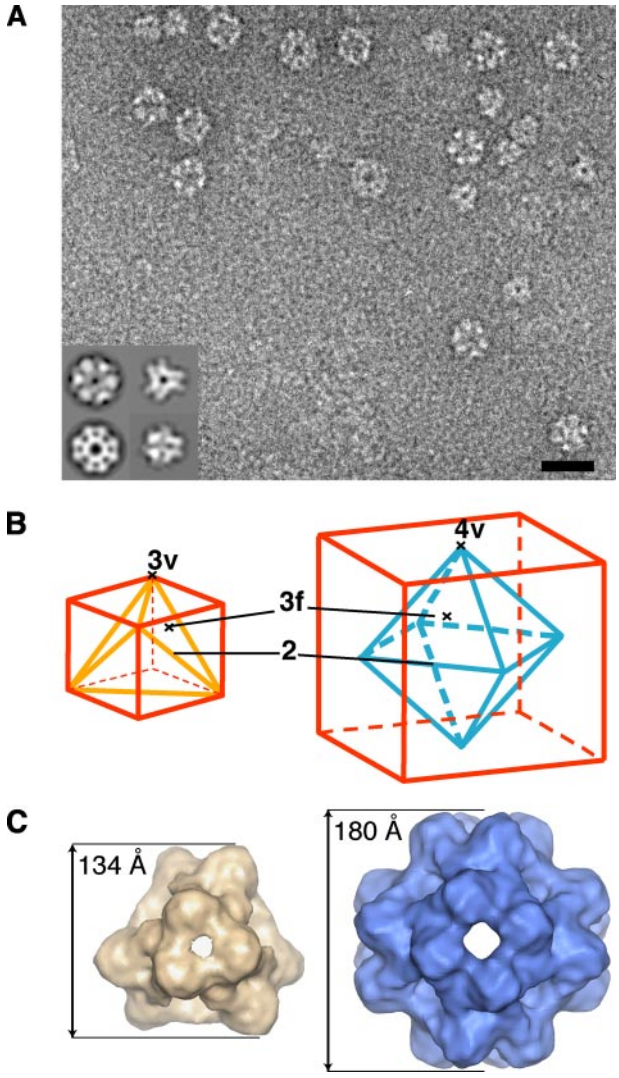

FIGURE 1. **Electron microscopy of PhTET1.** *A*, image in negative stain (sodium silicotungstate) of PhTET1 showing two types of particles. *Bottom left*, two-dimensional averages of 20 characteristic views of the large and the small particles. The large particle exhibits 3-fold (*top*) and 4-fold (*bottom*) symmetry axes. The small particle is similar to HmTET (15). The *scale bar* represents 20 nm. *B*, schematic views of a tetrahedron and an octahedron inscribed in a cube. The symmetry axes are indicated and called 3v or 3f for 3-fold on the vertex and on the facet, respectively. The abbreviation 4v is for 4-fold symmetry axis on the vertex. *C*, *left panel,* three-dimensional reconstruction of PhTET1-12s at 14 Å resolution viewed down the 3-fold symmetry axis on the vertex (3v); the diameter of the particle is 134 Å. *Right panel,* three-dimensional reconstruction of PhTET1-24s at 15 Å resolution viewed down the 4-fold symmetry axis on the vertex (4v); the diameter of the particle is 180 Å.

situated in each face of the tetrahedron, and four 15 Å pores (3v) are located at each vertex (Fig. 1, *B* and *C*). The tetracosameric assembly is a hollow octahedron that occupies a spherical volume of 180 Å diameter. Two types of holes penetrate the particle: six openings of 25 Å diameter at the vertices or 4-fold symmetry axes of the octahedron (4v) and eight orifices of 20 Å diameter in the center of the facets or 3-fold symmetry axes of the octahedron (3f) (Fig. 1, *B* and *C*).

Topology of the PhTET1 Subunit—We crystallized the 12-subunit tetrahedral complex. The three-dimensional structure of PhTET1-12s was solved at 3.1 Å resolution by molecular replacement, using the 1.9 Å resolution model of

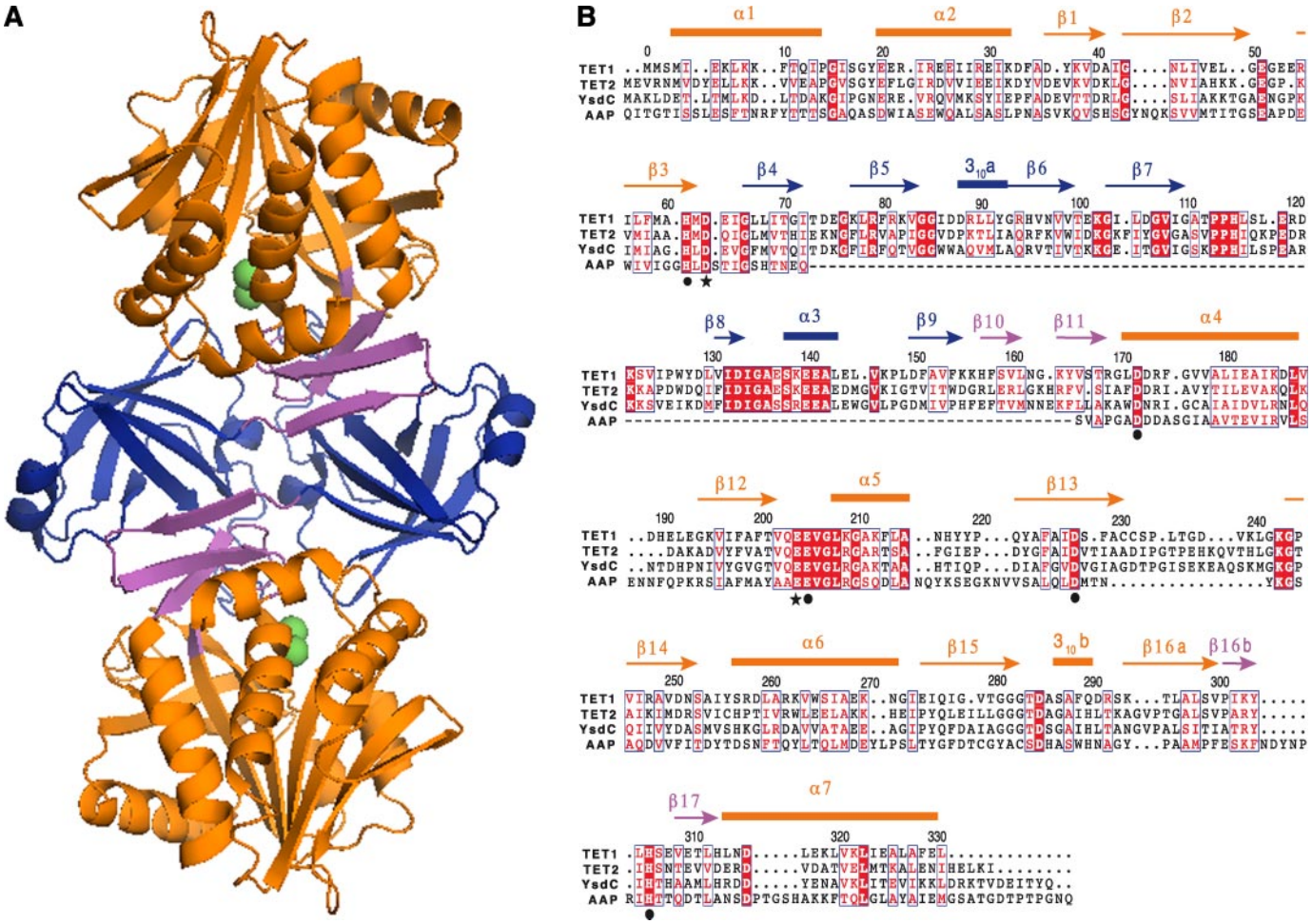

FIGURE 2. **Secondary structure elements of PhTET1.** *A*, schematic representation of the PhTET1-12s dimer along the 2-fold symmetry axis, as it appears viewed from the exterior of the dodecameric complex (see Fig. 3*A*, *left*). In each monomer, catalytic domains are colored in *orange* and *magenta,* dimerization domains in *blue,* and cobalt ions in *green.* Dimerization is achieved through formation of contacts between the dimerization domain of one monomer and a mixed four-stranded β-sheet (*magenta*) present in the catalytic domain of the other monomer. *B*, multiple sequence alignment indicating the secondary structure elements in PhTET1, assigned with DSSP (38), colored as in *A*. The abbreviations and GenBank™ accession numbers of the sequences are as follows: *TET1*, *P. horikoshii* TET1 (AP000002); *TET2*, *P. horikoshii* TET2 (AP000006); *YsdC*, *B. subtilis* YsdC protein (Z75208, Z99118); and AAP, aminopeptidase Ap1 from *Vibrio proteolyticus* (M85159, Z11993). The conserved metal-binding residues are indicated by a *ball* and the catalytic residues by a *star* (according to the MEROPS data base assignment).

the monomer from the homologous *B. subtilis* protein YsdC[7] (Protein Data Bank code 1VHE) as the search probe. The crystal asymmetric unit contains one monomer of PhTET1 of ~37 kDa. The electron density maps showed no density for the first two N-terminal SeMet residues; the model thus includes only the 330 C-terminal residues of the polypeptide. The subunit is a wedge-shaped parallelepiped of dimensions ~71 × 47 Å, arranged in two well separated domains (Fig. 2*A*) as follows: (i) a larger catalytic domain, comprising residues 2–65 and 156–331, and (ii) a smaller dimerization domain (residues 66–153).

The catalytic domain is a flattened globule with the topology of a three-layer αβα sandwich arranged around a central, mixed eight-stranded β-sheet (Fig. 2*A*, *orange*). In addition, a supplementary mixed four-stranded β-sheet formed by strands β10, β11, β17, and the bent C-terminal end of strand β16 (β16b) of the central β-sheet (Fig. 2*A*, *magenta*) is present at the periphery of the catalytic domain, adjacent to the smaller dimerization domain. This additional motif interacts with the dimerization domain of a second subunit to form the dimer (Fig. 2*A*; supplemental movie 1). Using the coordinates for the catalytic domain only, a similarity search for other three-dimensional structures using the protein structure comparison server SSM (36) returned a positive match to the three-dimensional structure of AAP (37). The amino acid sequence alignments of PhTET1, PhTET2, *Bacillus subtilis* YsdC, and AAP are shown in Fig. 2*B*. AAP lacks almost all the elements of the dimerization domain, in agreement with its monomeric organization. A three-dimensional structure superposition between the 0.95 Å resolution model of AAP (Protein Data Bank code 1RTQ) and the PhTET1 subunit gives a root mean square difference of 1.08 Å for 138 equivalent pairs of α-carbon. This confirms the postulated structural similarity between PhTET1 and clan MH aminopeptidases (39).

The crescent-shaped dimerization domain (Fig. 2*A*, *blue*) has a mostly β-barrel topology. It is made up of a six-stranded antiparallel β-barrel, completed by two helical segments on the outside of the barrel. The antiparallel β-barrel and one of the helices form the body and one of the tips of the crescent. The other tip is formed by the second helix and by a

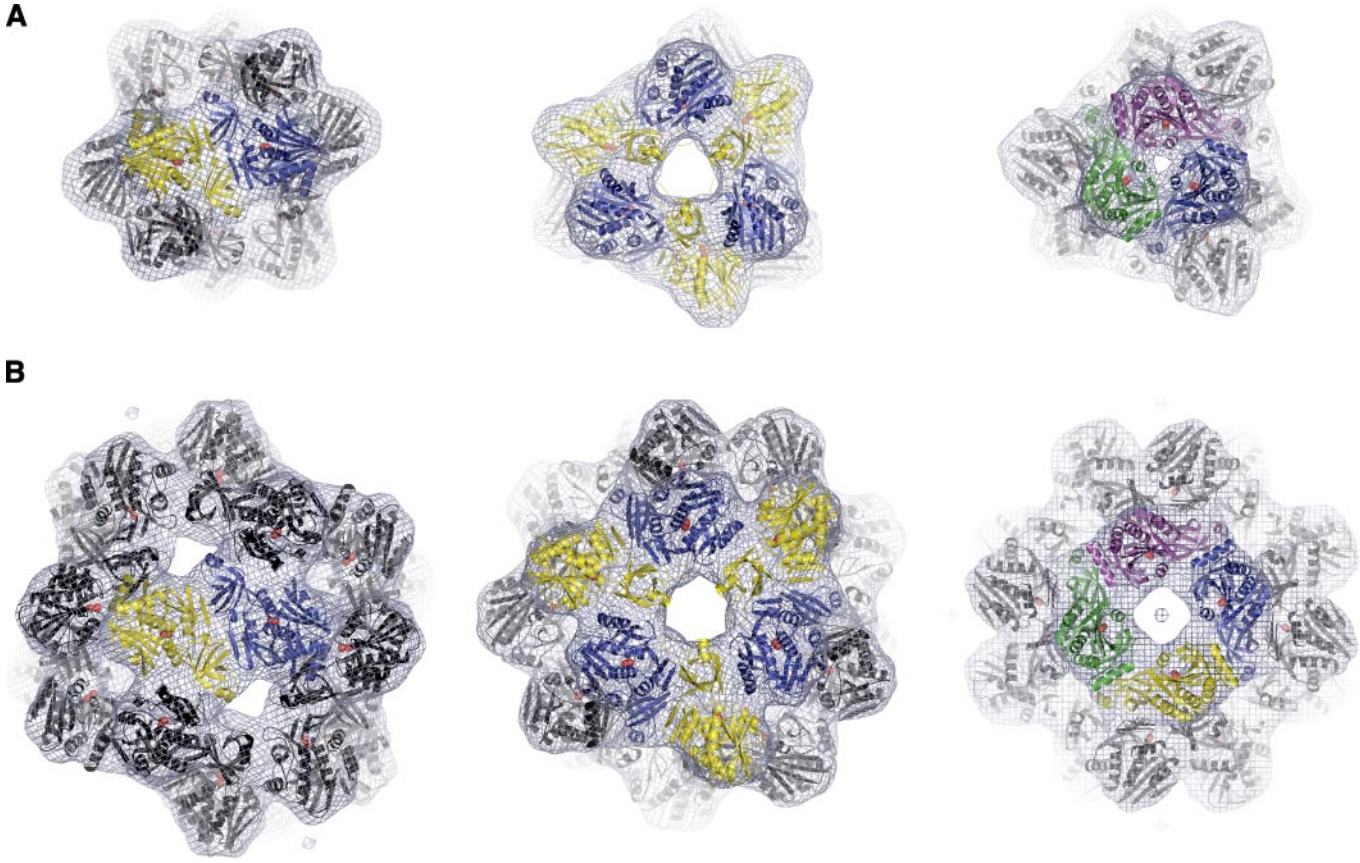

FIGURE 3. **Atomic and quasi-atomic model of the two PhTET1 particles.** *A*, atomic model of the PhTET1-12s complex, as determined by x-ray crystallography, fitted as a dodecamer into the EM envelope. From *left to right*, the edifice is viewed down 2-fold and two opposite sides of 3-fold symmetry axes. The EM envelope is depicted as a *mesh*, and the cobalt ions are represented by *red spheres*. The interactions between two monomers on the 2-fold symmetry axis (*left*), between six monomers on a facet (*middle*), and between three monomers on a vertex of the particle (*right*) are shown. *B*, quasi-atomic model of the PhTET1-24s particle depicting the 24 monomers fitted into the EM envelope. From *left to right*, the assembly is viewed down 2-, 3-(facet), and 4-fold (vertex) symmetry axes. The EM envelope and cobalt ions are represented as in *A*. The monomers interacting on the 2-, 3- and 4-fold symmetry axes are highlighted.

disordered loop (residues 111–130), where discontinuous electron density is observed for residues 115–122.

The initial difference electron density map showed, in the active site region, a very large positive density feature. This was interpreted as caused by the presence of metal ions in the active site. With divalent cobalt present in the crystallization solutions, the positive density disappeared when two divalent cobalt ions were modeled. The metal ligands are identical to those present in AAP (37) and PhTET2 (19, 20), with an identical type of coordination. Therefore, the catalytic mechanism of hydrolysis by AAP, PhTET2, and PhTET1 should be extremely similar, if not identical (19, 20, 40).

The tertiary structures of PhTET1 and PhTET2, although very similar, are not identical. PhTET2 has 22 amino acids more than PhTET1, and consequently, there are several secondary structure elements in PhTET2 that are not found in PhTET1. In particular, and following the assignment of Russo and Baumann (19), PhTET2 contains five 3_{10} helices (η1, η2, η4, η5, and η6), one loop (between η3 and β6), and one β-strand (β15) more than PhTET1. Moreover, the 3_{10}b helix in PhTET1 is an α-helix (α7) in PhTET2, and some common elements are formed by a different number of amino acids.

The crystal structure of PhTET2 contains an S1 hydrophobic specificity pocket adjacent to the metal-binding site (20), which explains the preferential activity of this aminopeptidase on peptides having an N-terminal hydrophobic or noncharged residue (18). The PhTET2 specificity pocket is lined with side chains of Ile^{238}, Leu^{293}, Thr^{237}, Glu^{291}, Lys^{261}, Ile^{322}, and Gly^{296}. Part of this pocket (Leu^{293}, Ile^{238}, and Gly^{296}) is involved in the binding of the inhibitor amastatin (20). The corresponding pocket in PhTET1 is constituted by the stretch Gly^{280}–Gly^{281}, the guanidinium moiety of Arg^{248}, and the main chains of Phe^{229}, Ala^{230}, and Thr^{280}. It is therefore less hydrophobic than the PhTET2 specificity pocket. In the dodecameric particle, this region of the active site also includes residues 114–118, belonging to the disordered loop of another subunit, which form a positively charged patch. These differences in the active site pockets and subpockets can account for the differences found in the substrate specificity for the two enzymes (see Refs. 21 and 18; see below).

Quaternary Structures of PhTET1; the Subunits Can Assemble into Two Alternative Arrangements—The three-dimensional crystallographic model of the PhTET1-12s subunit was fitted into the cryo-EM density maps of the 12- and 24-subunit assemblies to obtain the quasi-atomic structures of the complexes (Fig. 3). The PhTET1-12s EM model at 14 Å resolution is identical to the crystal structure. Octahedra and tetrahedra are Platon solids that exhibit triangular facets related by a 2-fold symmetry axis. The difference between these two volumes is located on their vertices (4- and 3-fold symmetry axes, respec-

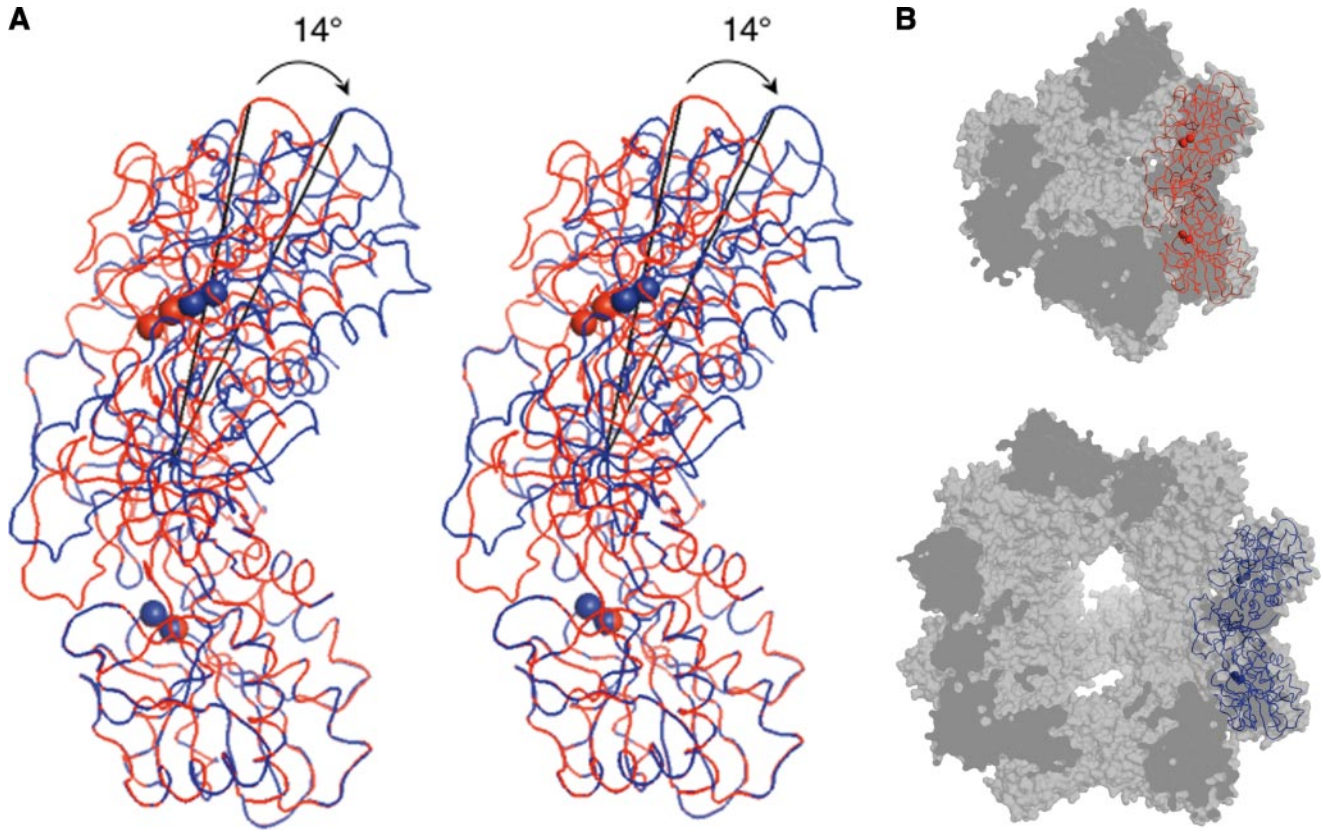

FIGURE 4. **Dimer structure in the two PhTET1 complexes.** *A*, ribbon representation of a dimer extracted from the tetracosamer quasi-atomic model (*blue*) superimposed to a dimer from the dodecamer x-ray structure (*red*). Cobalt ions are shown as *spheres*. The bottom monomers of each dimer were forced to match, hence the stereo picture illustrates the rotation of ~14° of the upper PhTET1-24s monomer with respect to the center of mass of the PhTET1-12s dimer. *A* and Fig. 2*A* are related by a 90° rotation around the vertical axis. *B*, cut open surface representations of the PhTET1 edifices showing the position of one dimer in the tetrahedral complex (*top*) and in the octahedral assembly (*bottom*). The dimers are depicted and oriented as in *A*.

tively; Fig. 1*B*). The building blocks used to generate both types of particles can therefore either be dimers (lying on each edge) or trimers (forming each faces of the tetrahedron or octahedron). The atomic structure of the tetrahedron and the calculated quasi-atomic model of the octahedron show that each facet is generated using a combination of six monomers (Fig. 3; supplemental movies 1 and 2). The building block for both structures is thus more likely to be the dimer.

On each tetrahedron vertex (3v), three subunits are arranged as trimers in a circular fashion. The junction found in each trimer delimits the smallest of the two types of holes present in the particle (Fig. 3*A*, *right*). The distance between the OH group of the successive Tyr^{219} residues situated at the border of the hole is ~7 Å. On the tetrahedron faces (3f), wider openings (~13 Å between the O-δ2 atoms of successive Asp^{74} residues) are located at the junction between six subunits (Fig. 3*A*, *middle*). These faces appear to be similar to those of the octahedron (Fig. 3*B*, *middle*). However, in the octahedral particle, the association that defines the apex small holes involves four PhTET1 monomers instead of three (Fig. 3*B*, *right*). The consequence is the generation of six wider (20 Å) novel types of openings (4v).

PhTET1 Assembles into Tetrahedral and Octahedral Particles Using Quasi-equivalent Contacts That Are Reminiscent of Those Found for Virus Capsids—In the two different quaternary arrangements of PhTET1, the dimeric building blocks are situated across the 2-fold symmetry axes, forming the assembly edges. Nevertheless, these building blocks are differently structured in the octahedral and the tetrahedral particles (Fig. 4). A rotation of ~14° of one of the monomers forming the dimer with reference to the center of mass of the PhTET1-12s dimer is evident in the building block of the tetracosameric assembly (Fig. 4*A*). In the two types of PhTET1 particles, the interactions between monomers to form the dimer involve the dimerization domain plus the four-stranded β-sheet present at the surface of the catalytic domain, which face each other in a head to tail fashion (Fig. 2*A*). However, the rigid body fitting of the PhTET1-12s monomer into the EM PhTET1-24s structure shows that the dimer making up the octahedron contains fewer contacts between the two monomers. In particular, strands β5, β14, and β15 participate in dimerization in the PhTET1-12s building block, but they do not seem to contribute to any intermonomer contact in the dimer from the 24-subunit complex. This allows the 14° rotation, which tilts one monomer with respect to the other.

This rotation has two important consequences. First, since the angle between the dimer monomers decreases in the side oriented toward the exterior of the particle (Fig. 4*B*), the resulting dimers when positioned in the final complex give rise to wider apex holes, allowing the insertion of a new dimer. This modification changes the geometry of the particle from tetrahedral to octahedral, and doubles the number of subunits of the assembly. The insertion of the new dimer is

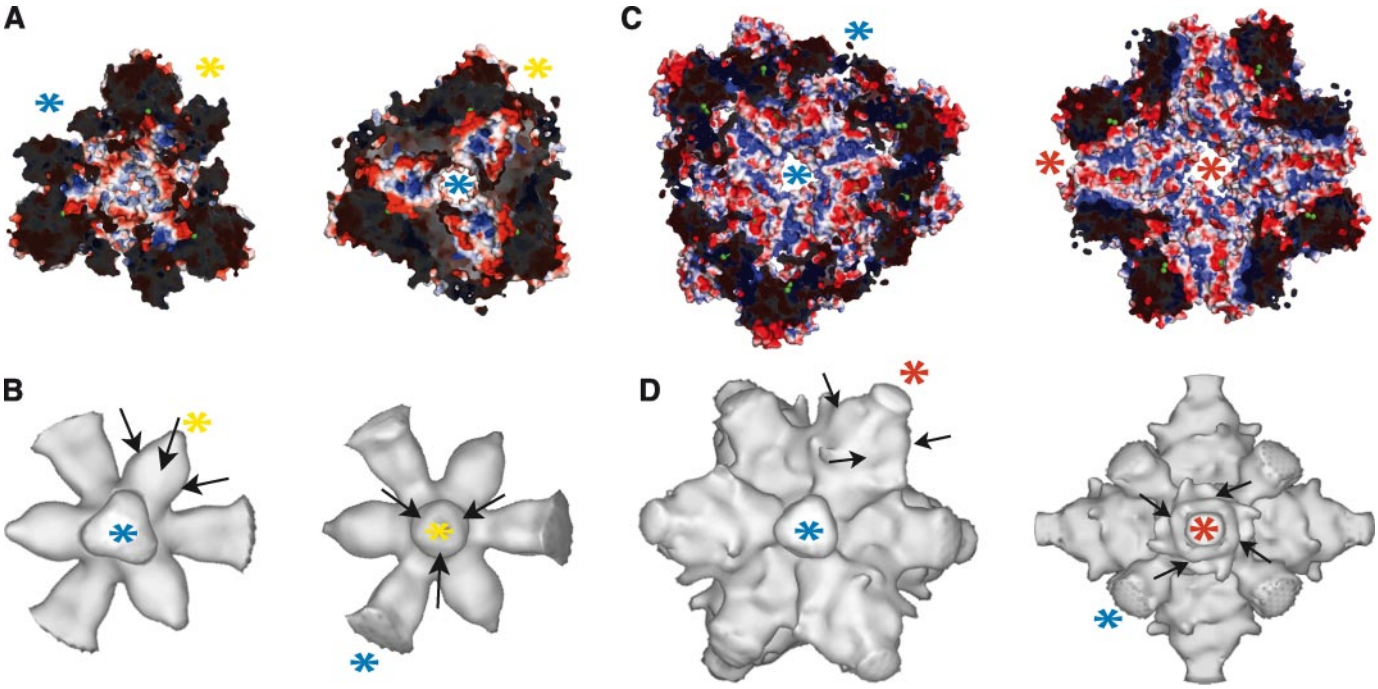

FIGURE 5. **Inside the PhTET1 complexes.** *A*, two halves of the tetrahedral edifice in cut-open surface representation. The particle surface is color-coded according to its electrostatic potential contoured from −5 kT/e (*intense red*) to +5 kT/e (*intense blue*) computed at 363 K, pH 7, 150 mM ionic strength, with a solute dielectric of 2 and a solvent dielectric of 80. The assembly is viewed down an access channel leading into the positively charged catalytic chamber (*left*) and in the opposite sense (*right*). Cobalt ions are colored in *green*. *Blue* and *yellow stars* are used to indicate where large (3f) and small (3v) openings, respectively, are situated. *B*, representation of the interior void volume of the dodecameric complex as obtained from the electron microscopy three-dimensional reconstruction. *Arrows* indicate the position of three active sites in a catalytic chamber. The orientations of the figures and the star codes are the same as in *A*. *C*, two halves of the quasi-atomic model of the octahedral edifice in cut-open surface representation viewed down the 3-fold (*left*) and the 4-fold (*right*) symmetry axes. The particle surface and cobalt ions are color-coded as in *A*. *Blue* and *red stars* indicate, respectively, where facet (3f) and vertex (4v) openings are located. *D*, representation of the interior void volume of the tetracosameric complex as obtained from the electron microscopy three-dimensional reconstruction. *Arrows* locate the active sites in a catalytic chamber. The orientations of the figures and the star codes are the same as in *C*.

possible because of a second change in the inter-subunit contacts. In the dodecameric particle, the formation of the trimer situated at the apex of the complex is achieved by interactions involving helices α2, α3, and α5 and strands β1, β4, and β5 from one PhTET1 subunit, and helices α6 and 3_{10}b and strands β14, β15, and β16a from the adjacent subunit. In the rigid body fitted tetracosameric particle, fewer contacts are again observed, because helices α2, α5, and 3_{10}b and strands β1, β5, β14, and β16 do not interact to form the apical tetramer. Instead, a new contact appears to be formed in which the loop between strands β4 and β5 is implicated (not shown). To date, quasi-equivalent contacts have been mainly found in icosahedral viral particles.

The second consequence of the 14° rotation is caused by the relative movement away from the catalytic domain of one monomer and the oligomerization domain of the other that results in a wider access to the active site in the octahedral particle (Fig. 4*B*). This improved accessibility probably has a direct effect on the catalytic properties of the complex. This issue is currently being studied in our laboratory.

Comparison of the position and type of the inter-subunit contacts that lead to dimerization in PhTET1-12s and in PhTET2 reveals that dimer formation is not achieved in the same way in the two molecules. In particular, a cluster of interactions is present in PhTET2 that is very different in PhTET1-12s (supplemental Fig. 2). There, only one interaction (hydrogen bond or salt bridge) is found, which connects Lys^{77} in strand β5 from one subunit to Lys^{303} in strand β16b from the other subunit. This interaction is not present in the PhTET1-24s dimer. The PhTET2 cluster is situated at the periphery and is repeated twice per dimer. It includes interactions that link the loop between strands β4 and β5 (following the assignment of Russo and Baumann, see Ref. 19) and strand β8 belonging to one subunit to the loop between strand β13 and helix η5, and the loop between strands β17 and β18 from the other subunit. This cluster contains numerous hydrophobic interactions, hydrogen bonds, and also a cation-electron π interaction. Therefore, its existence may lead to a higher rigidity of the PhTET2 dimer that could prevent the relative displacement of one monomer with respect to the other.

The PhTET1 Tetrahedral and Octahedral Particles Define a Network of Access Channels and Catalytic Chambers—The examination of the PhTET1-12s interior revealed a complex compartmentalization. The four large openings (3f) situated in each face of the tetrahedron give access to four wide channels that cross each other in the middle of the particle (Fig. 5, *A* and *B*; supplemental movie 1). Four funnel-shaped sub-compartments are enclosed in the apices of the complex and extend those channels (Fig. 5, *A* and *B*). These compartments are catalytic chambers each containing three active sites. Note that, with the exception of the active site pocket, the ~23 Å-long catalytic chamber is highly basic compared with the channels that are more contrasted regarding the charge of the surfaces. The four funnel-shaped catalytic chambers open up to the exte-

TABLE 1

Activity of PhTET1 on different peptides

Substrate peptides were used at a 5 mM initial concentration. Generation of products was quantified by reversed phase HPLC (see "Experimental Procedures").

Substrate	Product	PhTET1-12s		PhTET1-24s	
		At 5 min	At 25 min	At 5 min	At 25 min
		mmol of product/g of enzyme			
Asp-Ala	Asp	0.60	3.0	0.24	1.18
	Ala	0.60	2.8	0.26	1.24
Ala-Ala	Ala	3.5	17.3	8.5	43
Ala-Ala-Ala	Ala-Ala	24.1	138	20.0	100
	Ala	24.3	149	20.4	141
Ala-Ala-*p*NA	Ala-*p*NA	38	81	22.5	46
	pNA	0	0	0.13	0
Ala-Ala-Ala-*p*NA	Ala-Ala-*p*NA	38	170	15.9	60
	Ala-pNA	0.54	9.9	0.15	3.7
	*p*NA	0	0	0	0

rior by the narrow holes situated at each apex. These pores are not wide enough to allow the easy passage of an extended peptide. Accordingly, these orifices appear well adapted for the expulsion of the free amino acids generated by the aminopeptidase reaction.

Each 3f channel consists of three electrostatic layers (Fig. 5*A*, *left*) as follows: 1) a mixed entrance layer comprising the side chains of Asp^{74}, Glu^{75}, and Lys^{240}; 2) a positively charged layer formed by the side chain of Arg^{79}; and 3) a negatively charged layer composed of the side chains of Glu^{119} and Asp^{129}. These channels are ~15 Å long (channel length is defined as the distance between the O-δ2 atom of Asp^{74} and the Asp^{129} O-δ1). The channel intersection gives rise to a basic "spherical" central layer, which consists of the side chain of Lys^{122}. From there, the positively charged catalytic chambers can be accessed. These compartments are lined by the side chains of Arg^{120}, His^{115}, Asn^{252}, and Lys^{212}. On the way to the small apical hole (Fig. 5*A*, *right*), a negatively charged layer formed by the side chain of Asp^{291} appears before the final exit mixed layer composed of the side chains of Asn^{216} and Tyr^{219}. All the residues are repeated three times per circular layer, because the channels and catalytic chambers are at the interface between three PhTET1 subunits, except for the central layer in which the 12 Lys^{122} of the structure are present.

In the octahedral particle, the number of holes situated in the facets (3f) is doubled compared with the TET1-12s particle. Although these orifices have a triangular shape similar to that found in the dodecameric complex, the quasi-atomic model of the octahedral edifice shows that they are different. The octahedral-type organization of the subunits moves some acidic areas, placed on the surface of the tetrahedral complex, toward the inside of the particle. Hence the entrances become negatively charged (Fig. 5*C*; supplemental movie 2). In the channels to which these holes give access, the first two layers appear to be very similar to layers 1 and 2 of the dodecameric particle. However, unlike the 12-subunit complex, beyond these two layers the channel opens to a vast central cavity (~900 nm^3), which would contain alternating positive- and negative-charged areas formed by combination of layer 3, the central layer, and part of the catalytic compartment described above.

The PhTET1-24s complex holds six catalytic chambers (each containing four active sites) that form wide dome roof-like structures where the active sites are organized as a ring (*arrows* in Fig. 5*D*). These catalytic compartments are mostly positively charged like those observed in the dodecameric edifice (Fig. 5, *A* and *C*). However, in the tetracosameric complex they are broader and open to the exterior through wider orifices (20 Å).

The Octahedral PhTET1 Particle Is Catalytically Active—Unlike the PhTET2 protein (18), PhTET1 activity cannot be detected by using chromogenic aminoacyl compounds (AMC or *p*NA), probably because the X-AMC and X-*p*NA molecules cannot fit into the active site pocket or because these compounds fit but are not hydrolyzed. In fact, HPLC analysis of Ala-Ala-*p*NA degradation by the two PhTET1 oligomers showed that the generation of Ala-*p*NA was not linear with time (Table 1), suggesting product inhibition. Moreover, PhTET1 can cleave the N-terminal amino acid of larger peptides, even when the *p*NA moiety is in the C-terminal position, and can also hydrolyze dipeptides like Ala-Ala or Asp-Ala (Table 1). Therefore, PhTET1 seems to be unable to cleave a peptidic bond when *p*NA or AMC is in the P1′ position, making activity assays difficult.

PhTET1-12s enzymatic behavior has been partially characterized by Ando *et al.* (21). As they described, PhTET1-12s activity increases with substrate chain length (Table 1). However, unlike their results, we found no hydrolytic activity toward *N*-acetyl-Leu-*p*NA (*i.e.* deblocking activity). No *p*NA was detected by spectrophotometric analysis, and no *N*-acetyl-Leu, Leu-*p*NA, nor *p*NA could be measured by reversed phase HPLC. The same applies to the compound *N*-succinyl-Ala-Ala-*p*NA, because no Ala-Ala-*p*NA, Ala-*p*NA, nor *p*NA could be detected in the reaction mixture after a long incubation with PhTET1-12s. Comparable results were obtained when the deblocking activity of TET1–24s was assayed. Therefore, the deblocking activity of the enzyme, if present, is very low, and consequently the name DAP (for deblocking aminopeptidase) is ill suited to PhTET1.

The two PhTET1 oligomeric forms are similar with respect to their activity, but some differences exist. The dodecameric complex was in general more active than the 24s-subunit edifice (Table 1). Among the assayed compounds, Ala-Ala-Ala-*p*NA was found to be the best substrate for PhTET1-12s, whereas the tetracosameric complex showed maximal activity against Ala-Ala-Ala and Ala-Ala-*p*NA.

DISCUSSION

The quaternary structures of PhTET1 described in this paper reveal a novel type of elaborated self-compartmentalized orga-

nization for a peptidase complex. Both versions of the edifice (PhTET1-12s and PhTET1-24s) are structured in a related fashion with two types of subcompartments: the entry channels (4 and 8, respectively) and the proteolytic chambers (4 and 6, respectively). However, the dodecamer is more compact than the tetracosamer.

The tetrahedral organization of PhTET1-12s indicates a function as a peptide scavenger, the geometry and electrostatic charge repartition in the channels being involved in the substrate peptide binding and orientation toward the catalytic chambers. The channel dimensions are in the same range as those described for barrel-shaped peptidases that process unfolded polypeptides such as the 20 S proteasome (41) and ClpP (42), and are large enough to let even partially folded polypeptides (such as single helices or helical coils) enter the particle. The succession of positively and negatively charged patches present on the surface of PhTET1-12s channels would trigger the translocation of the polypeptides toward the catalytic chambers by maintaining the substrate (also containing different types of charged areas) in continuous motion. By contrast, the catalytic chambers are highly positively charged with the exception of the active sites. This feature would facilitate a greater mobility of the substrate N-terminal extremity, when it enters the catalytic compartment, because of the electrostatic repulsion, and thus would permit a flip to one of the three highly acidic bi-metallic active sites. The catalytic chambers provide a high concentration of active sites located on the same plane. Note that these compartments have a funnel-like shape that could prompt the ejection of the released free amino acids by the nearby narrow pore located at the apex of the complex (Fig. 5, *A* and *B*). The strong negative charge created by the aspartate residues (Asp^{291}) preceding the apex openings could serve to attract the positively charged N termini of the generated amino acids, which could be then hooked up by the tyrosine residues (Tyr^{219}) surrounding the apex holes. In fact, if an alternate conformer of the side chains of these residues is taken (together with an alternate conformer for the side chain of Asp^{291} that does not provoke steric clashes with the remainder of the polypeptide), the exit hole becomes wider with ~16 Å between the C-β positions of two successive Tyr^{219} side chains (supplemental Fig. 3). This tyrosine side chain swing would allow the transfer of the free amino acid to the exterior, providing a product ejection mechanism. The organization of the quaternary structure of the PhTET1-12s particle thus appears to be optimal for the elimination of the N-terminal residue from a polypeptidic chain.

The mechanism of substrate navigation based on the highly compartmentalized nature of PhTET1-12s and on its surface electrostatic potential features is clearly different from that proposed for PhTET2 (20). Such a discrepancy in the putative mode of action of the two peptidases could be explained by the differences in their respective quaternary structures. The PhTET2 particle encloses an internal cavity that appears to be an open space harboring all the catalytic sites. PhTET2 does not contain catalytic chambers as those described for PhTET1. The apices of the PhTET2 complex are almost closed, and three small holes, which were proposed to be the exit channels of the generated free amino acids, are disposed around the pore situated in the facets of the complex (20). Those three small holes, each of which is connected directly to one active site, do not exist in the PhTET1 edifices. Consequently, despite their apparent similarity, the two peptidases have specific features regarding their quaternary structures and mode of action. Note that the enzymatic properties of the different TET proteins characterized to date are not identical; HmTET is a broad aminopeptidase (15); PhTET2 acts preferentially on neutral N-terminal residues (18), and PhTET1 is unable to cleave a peptide bond when *p*NA or AMC is in the P1′ position and seems to exhibit a narrow specificity.[8] Nevertheless, the apical holes of the PhTET2 dodecameric complex are lined by the side chains of three phenylalanine residues (20), which could undergo a swing similar to that described for the tyrosine residue side chains in PhTET1-12s. Because PhTET2 acts preferentially on aliphatic N-terminal amino acids, a releasing strategy involving hydrophobic interactions between the side chain of the cleaved amino acid and the phenylalanine aromatic ring seems possible. In this case, the mechanisms of substrate channeling and processing, and also of product release by the two TET peptidases, would be comparable, and differences regarding the substrate specificity would be easily explainable considering the divergences existing in their specificity pockets. Although the TET peptidases can break down large peptides into free amino acids (15, 18, 21), the process is not sequential, as we demonstrated for PhTET2 (18). The lack of processivity is evident also from the analysis of Table 1, because degradation of the longest peptides involves the accumulation of shorter intermediary peptides, although they are substrates (*e.g.* Ala-Ala, Ala-Ala-*p*NA). Therefore, the peptide moiety is detached from the active site once the N-terminal residue has been cleaved, probably to allow the discharge of the free amino acid.

The Tricorn proteases (TRI) are another type of large proteolytic complex generally present in archaeal lineages where TET-like peptidases are absent. It is thus quite likely that the two systems represent functional homologs. Tricorn activity generates di- and tripeptides, and hence, the synergistic action of three aminopeptidase factors is needed to yield free amino acids (43). Biochemical studies have suggested that this modular proteolytic system would work in synergy with the proteasome (44). TRI assembles as a 720-kDa complex that is composed of six identical copies of a 120-kDa polypeptide. Despite an apparent similarity between the external shapes of the TET and TRI complexes (20), the PhTET1 structure examination reveals a completely different internal organization. The Tricorn particle is a flattened complex that encloses six active sites in a central cavity, which is accessible by two main holes (44). In the case of PhTET1 there is no cavity *per se* but a network of channels and catalytic chambers.

A striking feature of PhTET1 is its ability to assemble into two different quaternary structures, involving quasi-equivalent contacts between monomers. In viruses, this characteristic can

[8] M. A. Durá and B. Franzetti, unpublished results.

result not only in differences in the contacts among capsomers in one viral particle but also in the formation of several sized particles. For example, the hepatitis B core particle can assemble into $T = 4$ or $T = 3$ particles comprising 120 and 90 dimers, respectively (45). The PhTET1 edifices represent the first nonfilamentous and nonviral objects where the same kind of phenomena are found. Although Tricorn can form a giant icosahedral capsid, this assembly consists of 20 copies of the 720-kDa TRI complex (46), and therefore it does not imply any change in the contacts between monomers composing the TRI hexamer.

What is the role of a giant hollow octahedral peptidase, larger than the 20 S proteasome, within the cells? We have shown that the PhTET1-24s particle is nearly as active as the dodecameric form. The biological relevance of such an alternative way of assembly remains unknown. At this stage, one can only propose that a more expanded quaternary structure would facilitate the trapping of small peptides (2–6 residues) and may facilitate their free diffusion toward the active sites. The more compact, channeled tetrahedral complex would be a complementary system, streamlined for the processing of longer polypeptides because of its better capacity to guide them toward the catalytic chambers. PhTET1-12s together with PhTET2 could therefore be responsible for the complete breakdown of 6–20-residue proteasomal products, whereas PhTET1-24s could be involved preferentially in the nutritional pathway by hydrolyzing small peptides imported from the external environment. This hypothesis is supported by the fact that Pyrococcales are proteolytic Archaea and that complete DNA microarray data from *Pyrococcus furiosus* have shown that the gene encoding for a TET1 homologous protein is dramatically up-regulated in peptide-grown cells (47). Furthermore, the fold of the catalytic domain of PhTET1 resembles that of AAP and *Streptomyces griseus* aminopeptidase (48), two peptidases from family M28 in clan MH. This family contains several bi-metallic secreted aminopeptidases. All of them are monomeric. In the case of the TET peptidases, the dimerization domain was probably added subsequently during evolution to prevent unwanted proteolytic damage, allowing their cytosolic localization.

Acknowledgments—We thank ID14-4 beam-line staff at the European Synchrotron Radiation Facility (Grenoble), Rémi Pinck (EMBL-Grenoble), and Jacques-Philippe Colletier (Laboratoire d'Enzymologie Moléculaire-Institut de Biologie Structurale) for computational support; Dr. Elizabeth Hewat (Laboratoire de Microscopie Electronique Structurale-Institut de Biologie Structurale) and the Institut de Biologie Structurale for the use of the Philips CM200 cryomicroscope and image scanner; Jean-Pierre Andrieu (Laboratoire d'Enzymologie Moléculaire-Institut de Biologie Structurale) for amino acid analysis and computational support; and Dr. Richard H. Wade (Laboratoire de Microscopie Electronique Structurale-Institut de Biologie Structurale) for critical reading of the manuscript.

REFERENCES

1. Kirschner, M. (1999) *Trends Cell Biol.* **9,** M42–M45
2. Gottesman, S. (2003) *Annu. Rev. Cell Dev. Biol.* **19,** 565–587
3. Baumeister, W., Walz, J., Zühl, F., and Seemüller, E. (1998) *Cell* **92,** 367–380
4. Hershko, A., and Ciechanover, A. (1998) *Annu. Rev. Biochem.* **67,** 425–479
5. Sauer, R. T., Bolon, D. N., Burton, B. M., Burton, R. E., Flynn, J. M., Grant, R. A., Hersch, G. L., Joshi, S. A., Kenniston, J. A., Levchenko, I., Neher, S. B., Oakes, E. S., Siddiqui, S. M., Wah, D. A., and Baker, T. A. (2004) *Cell* **119,** 9–18
6. Kisselev, A. F., Akopian, T. N., Woo, K. M., and Goldberg, A. L. (1999) *J. Biol. Chem.* **274,** 3363–3371
7. Botbol, V., and Scornik, O. A. (1991) *J. Biol. Chem.* **266,** 2151–2157
8. Gonzales, T., and Robert-Baudouy, J. (1996) *FEMS Microbiol. Rev.* **18,** 319–344
9. Tamura, T., Tamura, N., Cejka, Z., Hegerl, R., Lottspeich, F., and Baumeister, W. (1996) *Science* **274,** 1385–1389
10. Burley, S. K., David, P. R., Sweet, R. M., Taylor, A., and Lipscomb, W. N. (1992) *J. Mol. Biol.* **224,** 113–140
11. Joshua-Tor, L., Xu, H. E., Johnston, S. A., and Rees, D. C. (1995) *Science* **269,** 945–950
12. Remaut, H., Bompard-Gilles, C., Goffin, C., Frère, J.-M., and van Beeumen, J. (2001) *Nat. Struct. Biol.* **8,** 674–678
13. Rockel, B., Peters, J., Muller, S. A., Seyit, G., Ringler, P., Hegerl, R., Glaeser, R. M., and Baumeister, W. (2005) *Proc. Natl. Acad. Sci. U. S. A.* **102,** 10135–10140
14. Yao, T., and Cohen, R. E. (1999) *Curr. Biol.* **9,** R551–R553
15. Franzetti, B., Schoehn, G., Hernandez, J. F., Jaquinod, M., Ruigrok, R. W., and Zaccai, G. (2002) *EMBO J.* **21,** 2132–2138
16. Rawlings, N. D., Tolle, D. P., and Barrett, A. J. (2004) *Nucleic Acids Res.* **32,** D160–D164
17. Gonzalez, J. M., Masuchi, Y., Robb, F. T., Ammerman, J. W., Maeder, D. L., Yanagibayashi, M., Tamaoka, J., and Kato, C. (1998) *Extremophiles* **2,** 123–130
18. Durá, M. A., Receveur-Brechot, V., Andrieu, J. P., Ebel, C., Schoehn, G., Roussel, A., and Franzetti, B. (2005) *Biochemistry* **44,** 3477–3486
19. Russo, S., and Baumann, U. (2004) *J. Biol. Chem.* **279,** 51275–51281
20. Borissenko, L., and Groll, M. (2005) *J. Mol. Biol.* **346,** 1207–1219
21. Ando, S., Ishikawa, K., Ishida, H., Kawarabayasi, Y., Kikuchi, H., and Kosugi, Y. (1999) *FEBS Lett.* **447,** 25–28
22. Porciero, S., Receveur-Bréchot, V., Mori, K., Franzetti, B., and Roussel, A. (2005) *Acta Crystallogr. Sect. F Struct. Biol. Crystalliz. Comm.* **61,** 239–242
23. Fabry, C. M. S., Rosa-Calatrava, M., Conway, J. F., Zubieta, C., Cusack, S., Ruigrok, R. W., and Schoehn, G. (2005) *EMBO J.* **24,** 1645–1654
24. Conway, J. F., and Steven, A. C. (1999) *J. Struct. Biol.* **128,** 106–118
25. Frank, J., Radermacher, M., Penczek, P., Zhu, J., Li, Y., Ladjadj, M., and Leith, A. (1996) *J. Struct. Biol.* **116,** 190–199
26. van Heel, M. (1987) *Ultramicroscopy* **48,** 95–100
27. Kabsch, W. (1988) *J. Appl. Crystallogr.* **21,** 916–924
28. Rossmann, M. G. (1972) in *The Molecular Replacement Method* (Rossmann, M. G., ed) Gordon and Breach Science Publishers, Inc., New York
29. Read, R. J. (2001) *Acta Crystallogr. Sect. D Biol. Crystallogr.* **57,** 1373–1382
30. Brünger, A. T., Adams, P. D., Clore, G. M., DeLano, W. L., Gros, P., Grosse-Kunstleve, R. W., Jiang, J. S., Kuszewski, J., Nilges, M., Pannu, N. S., Read, R. J., Rice, L. M., Simonson, T., and Warren, G. L. (1998) *Acta Crystallogr. Sect. D Biol.* **54,** 905–921
31. Laskowski, L. A., MacArthur, M. W., Moss, D. S., and Thornton, J. M. (1993) *J. Appl. Crystallogr.* **26,** 283–291
32. Baker, N. A., Sept, D., Joseph, S., Holst, M. J., and McCammon, J. A. (2001) *Proc. Natl. Acad. Sci. U. S. A.* **98,** 10037–10041
33. DeLano, W. L. (2002) *The PyMOL User's Manual,* DeLano Scientific, San Carlos, CA
34. Wriggers, W., and Birmanns, S. (2001) *J. Struct. Biol.* **133,** 193–202
35. Navazza, J., Lepault, J., Rey, F. A., Álvarez-Rúa, C., and Borge, J. (2002) *Acta Crystallogr. Sect. D Biol. Crystallogr.* **58,** 1820–1825
36. Krissinel, E., and Henrick, K. (2004) in *Acta Crystallogr. Sect. D Biol. Crystallogr.* **60,** 2256–2268
37. Chevrier, B., Schalk, C., D'Orchymont, H., Rondeau, J. M., Moras, D., and Tarnus, C. (1994) *Structure* (*Lond.*) **2,** 283–291
38. Kabsch, W., and Sander, C. (1983) *Biopolymers* **22,** 2577–2637
39. Onoe, S., Ando, S., Ataka, M., and Ishikawa, K. (2002) *Biochem. Biophys. Res. Commun.* **290,** 994–997
40. Stamper, C., Bennett, B., Edwards, T., Holz, R. C., Ringe, D., and Petsko, G.

(2001) *Biochemistry* **40,** 7035–7046
41. Löwe, J., Stock, D., Jap, B., Zwickl, P., Baumeister, W., and Huber, R. (1995) *Science* **268,** 533–539
42. Wang, J., Hartling, J. A., and Flanagan, J. M. (1997) *Cell* **91,** 447–456
43. Tamura, N., Lottspeich, F., Baumeister, W., and Tamura, T. (1998) *Cell* **95,** 637–648
44. Kim, J.-S., Groll, M., Musiol, H. J., Behrendt, R., Kaiser, M., Moroder, L., Huber, R., and Brandstetter, H. (2002) *J. Mol. Biol.* **324,** 1041–1050
45. Wingfield, P. T., Stahl, S. J., Williams, R. W., and Steven, A. C. (1995) *Biochemistry* **34,** 4919–4932
46. Walz, J., Koster, A. J., Tamura, T., and Baumeister, W. (1999) *J. Struct. Biol.* **128,** 65–68
47. Schut, G. J., Brehm, S. D., Datta, S., and Adams, M. W. W. (2003) *J. Bacteriol.* **185,** 3935–3947
48. Greenblatt, H. M., Almog, O., Maras, B., Spungin-Bialik, A., Barra, D., Blumberg, S., and Shoham, G. (1997) *J. Mol. Biol.* **265,** 620–636